SNO-STR-95-007: Optics and Geometry in the SNO Detector

T. J. Radcliffe

Department of Physics,
Queen's University at Kingston,
K7L 3N6, Canada

1 Introduction:

This paper describes attempts to correct events in the SNO detector for the effects of optics and geometry on the transmission of light from where it is created to where it is detected. Cherenkov light is created in approximately point-like events and propagated through the D_2O , the acrylic and the H_2O until it strikes a PMT/concentrator or other absorbing surface. Because the light is not created isotropically there are corrections for solid angle as well as optical attenuation and angular response of the PMT/concentrator combination. Due to these effects, the number of photons detected from an electron with a given energy will depend on the electron's position and direction. Naively (and, as it turns out, incorrectly) one might expect that accounting for these effects would result in improved detector resolution.

A considerable amount of background material has been omitted from this report, and will be described elsewhere. This includes detailed comparisons of the Queen's MC, the calibration MC and SNOMAN. A brief description of comparison of codes and optical data sets has been included to give an estimate of the reasonable range of optical properties – particularly for D_2O and H_2O – that might be encountered in the detector.

As one might expect, most of the work described here is tentative and incomplete, as many of the problems discussed are interdependent: Monte Carlo validation should be complete prior to detailed analysis, and the best fitter available should be used to fit events prior to optical correction. Also, optical properties that have been extracted from simulated data should be used to perform optical correction. As such, this report should be viewed as an outline of future work in which each section will be expanded into a

complete report. It should give some idea of the scope of the work facing us if we want to be able to analyze real data and assign realistic uncertainties to the results of that analysis.

The simulations for this work have been done with the calibration MC using SNOMAN optical properties. A forthcoming report will describe it in detail. Fitting of events was done with the modal fitter, also to be described elsewhere. Comparisons with SNOMAN were performed running SNOMAN on both a MIPS R4000 box and a SUN SPARC 10. The calibration MC was run exclusively on the MIPS R4000. It is important to remember in reading what follows that *the MIPS R4000 running RISCos 5.01 is known to have significant bugs in both the C compiler and the operating system kernel.* There are also known problems with the FORTRAN optimizer. Both SNOMAN and the calibration MC are mixed-language code (SNOMAN by virtue of its use of CERNLIB) and while the calibration MC has been extensively tested on this system (during which process the aforementioned kernel bug made itself known, and a work-around developed) SNOMAN has not. In any case, it is my opinion that all results from these machines should be considered suspect: amongst other work going on at Queen's currently is an attempt to understand very significant ($> 6\sigma$) differences between some of the SNOMAN outputs when run on an R4000 versus SNOMAN run on a SPARC 10.

2   Optical Data Sets:

Figures 1, 2 and 3 show absorption length in D_2O , acrylic and H_2O as a function of wavelength based on three different assumptions about the White Book attenuation data and the behaviour of acrylic. SNOMAN input data are shown in Tables 1, 2 and 3 as well. Remarkably, for D_2O , the input data for QMC are the most optimistic. The calibration MC inputs are based on the assumption that all of the White Book attenuation is due to absorption, and the SNOMAN inputs appear to favour the dominance of scattering at longer wavelengths.

Figure 2 shows that the three data sets agree quite well for acrylic at short wavelengths below 400 nm where absorption is most important. The calibration MC input data are in this case an average over the measurements of acrylic done by Davis Earle at Chalk River. Figure 3 shows that for H_2O the QMC inputs are once again the most optimistic, with SNOMAN and the calibration MC agreeing at short wavelengths but diverging in the 350 - 550 nm range. Differences where the absorption length is long, however, are relatively unimportant.

The refractive indices are assumed to be independent of wavelength in

2

QMC, and their variation with wavelength is quite similar in SNOMAN and the calibration MC. In all codes the number of Cherenkov photons is determined by an average refractive index of 1.34, but the angular distribution of the photons in the calibration MC is determined by the wavelength-dependent refractive index: this is a negligibly small effect compared to other problems with photon angular distributions discussed below.

3   Code Comparisons:

Three codes now exist that are capable of modeling the SNO detector. Each has its own strengths and weaknesses: QMC is very fast but the geometric modeling is incomplete (no neck, no thick panels, no joints) and in places incorrect (the concentrators are too long and have the wrong profile, and no PMT internal structure is included.) SNOMAN now has the most complete geometric model available by a wide margin, but is relatively large and slow: it takes 15 Mbytes of RAM to run, and runs about 3 times more slowly than the calibration MC and 10 times more slowly than QMC (this is for the default SNOMAN configuration as of 2.06, which means PMTs are simulated with grey discs and CERFAC is 0.22 – a more realistic comparison would by with 3D PMTs turned on.) The calibration MC is smaller (5 Mbytes at runtime) and somewhat faster, but uses a somewhat less realistic geometry for some components (concentrators and PMTs are modeled as combinations of spherical, ellipsoidal and paraboloidal surfaces) and the thick panels have incorrect edge shapes (no beveled edges) and no rope grooves. The calibration MC does include diffuse scattering off joints, which is currently being added to SNOMAN. Like SNOMAN, the calibration MC may be used with different levels of geometric complexity: for the simulations discussed in this report a simple geometry was used. All tests described in this paper deal with electrons only. Neither QMC nor the the calibration MC can deal with muons or neutrons (neutron capability may be added to the calibration MC at some future date.)

Code comparisons were done for several purposes: to ensure that the basic physics was in agreement in all cases, that the differences in geometry don't make too large a difference in the results (this is a strong measure of robustness) and that there were not any hidden parameter-sensitivities in the results.

3

Material	Simple	Calib	QMC
D_2O	0.69535	0.6881	-
Acrylic	0.77795	0.7860	-
H_2O	0.89242	0.8797	-
Geometry	0.63	0.63	-
Total	0.3041	0.2997	0.2900

Table 4: Optical Attenuation in MCs for Events at Centre Compared to Simple Calculation

3.1 Basic Physics

The basic physics appears to be in good agreement everywhere. The codes create about the same number of Cherenkov photons (when corrected for differing wavelength intervals) and propagate them consistently when given the same input parameters. For a 10 MeV isotropic electron source at the centre of the vessel it is simple to predicted the detector response, and there is good agreement between the simple calculation and the MC results. Table 4 shows the results of some comparisons between a simple calculation of detector response with black disks and the responses of QMC and the calibration MC. Because SNOMAN is still improving rapidly, and is still in the process of debugging, this comparison was not made with SNOMAN, although SNOMAN input values were used in all cases, allowing simple comparison at some future date.

3.2 Geometric Differences

The geometric differences between codes are quite complex. Three concentrator shapes are shown in Figure 4. As can be seen, the QMC shape differs markedly from the SNOMAN shape. In QMC the concentrator is also about 5 cm longer than the SNOMAN concentrator; this extra length is not shown, and none of the comparisons use it. Figure 5 shows the deviation between the shape used in the calibration MC and the shape used in SNOMAN.

Detailed comparisons were made between the SNOMAN PMT shape run in GMC and the data in Mike Lay's thesis. Initial agreement was extremely poor. However, making the photocathode finite thickness (it was originally modeled in GMC as an infinitely thin absorbing layer) and adding the internal PMT geometry (reflective coating, partially reflective dynode stack) improved the agreement considerably. The measured and calculated GMC response are shown in Figure 6, and as can be seen the difference between them is everywhere less than 5%. Given that GMC is still using a spherical

4

PMT envelope, agreement at this level is quite promising.

Based on this work it is highly probable that the geometric model of the PMTs used in QMC will result in substantially incorrect results for detector response to events in the H_2O , where the differences in concentrator response is largest. This will be investigated in more detail in future. The lack of internal geometry in the QMC simulation may also result in significant differences between PMT calculated and actual PMT response.

3.3 Parameter Dependencies

Finally, there is the question of what results, if any, depend on the input parameters. Some earlier work suggested that the circular Hough transform results were dependent on optical attenuation inputs (in particular, that the energy-independence of the pattern parameter was due to the use of QMC optical inputs) but this has not been pursued further. A more significant parameter dependence was found when generating data to produce a two-dimensional distribution of number of photons vs. energy and angle for doing optical correction. As shown in Figures 7 and 8, there is a significant difference in the number of photons emitted precisely at the Cherenkov angle for low-energy electrons as ESTEPE is wound down from 5% to 1%. ESTEPE is the EGS4 parameter that gives the maximum fractional energy loss of an electron in a single step. As ESTEPE decreases, so does the maximum allowed step length. As the multiple scattering correction to the electron's direction is put in at the end of the step, the electron travels in a straight line over the course of the step. This means that for large ESTEPE values for electrons near the Cherenkov threshold, a significant fraction of their Cherenkov photons will be generated relative to the initial direction, without any correction for scattering. For electrons far above threshold the effect is much smaller, but still noticeable.

There are two possible consequences of this parameter dependence: the first is that pattern recognition algorithms will work slightly better than they ought, even at high energy. The second, and perhaps more important effect, is that PMT β/γ events will have excess light emitted exactly on the Cherenkov cone of the initial electron direction (this is true for both the β and the electron from the γ. As light emitted on a perfect cone carries relatively little information when analyzed with a time fitter, this effect may play a role in the badly mis-reconstructed PMT β/γ events that leak into the central volume of the detector and contaminate the internal β/γ background measurements. As such, this phenomenon bears closer investigation, which will be undertaken in future.

5

E-mail discussion via the software group has resulted in the suggestion by Mike Lowry to include the generation of Cherenkov photons in the EGS4 logic. This possibility is being investigated for all three simulation codes. A simple fix has been put into the calibration MC: the electron direction is smoothly varied along the length of the step. This will give something close to the correct smearing in θ but will still leave the correlation in ϕ too large.

4 Correcting for Optics and Geometry

The following discussion is duplicated exactly in SNO-STR-95-002, and is included here to make this report self-contained.

The correction algorithm is equivalent integrating the Cherenkov photon distribution from an electron with a given position, direction and energy over all PMTs, including optical factors. This is just the calculation that is done by the Monte Carlos, so what we have is an analytic form of the Monte Carlo calculation. The only restriction is that we be concerned only with light that is "in-time" – i.e. unscattered and unreflected. With this restriction in place, the following algorithm can be used to determine the detector response independently of the Monte Carlo, which may be useful for modeling some higher-energy events, as the algorithm's speed is independent of the number of Cherenkov photons.

For an electron at time t with position $\vec{x}$, initial direction $\hat{u}$ and energy E the mean number of Cherenkov photons emitted into the solid angle of PMT i is:

$$N_e^i = \left[\frac{dN}{d\cos\theta} \right] \frac{r^2(-\hat{u}_p \cdot \hat{u}_i)}{2R^2} \tag{1}$$

where

$$\frac{dN}{d\cos\theta} = \text{angular distribution of emitted photons}$$
$$\theta = \text{angle between emitted photon and electron direction}$$
$$R = |\vec{x}_i - \vec{x}|(\text{distance from event position to PMT } i)$$
$$\vec{x}_i = \text{position of PMT } i$$
$$\hat{u}_p = \frac{\vec{x}_i - \vec{x}}{R}(\text{direction of optical photon})$$
$$\hat{u}_i = \text{inward direction of PMT}$$
$$r = \text{radius of the PMT/concentrator face}$$

6

The angular distribution of photons from the electron, $\frac{dN}{d\cos\theta}$, is a function of energy as well as angle: it is the number of photons emitted between $\cos(\theta - d\theta)$ and $\cos(\theta + d\theta)$ (where $d\theta$ is the half-angle subtended by the PMT) for an electron of energy E. This distribution is shown for an ESTEPE value of 0.01 for electrons in water in Figure 8.

The number of photons detected by the PMT depends on the absorption probabilities in the D_2O, the acrylic and the H_2O, as well as on the reflection probabilities at the water/acrylic interfaces and on the PMT quantum efficiency. Nominally, the probability of PMT i detecting a photon emitted toward it is:

$$P_d^i = \epsilon^i(l_{D_2O}, l_{acr}, l_{H_2O}) \times P_s \times (1 - P_{ri}) \times (1 - P_{ro}) \times \mathcal{R}(\hat{u}_p \cdot \hat{u}_i) \quad (2)$$

where

$$
\begin{aligned}
\epsilon(l_{D_2O}, l_{acr}, l_{H_2O}) \quad &= \quad \text{effective QE of PMT} \\
P_s \quad &= \quad exp(-l_{D_2O}/\lambda_{D_2O} - l_{acr}/\lambda_{acr} - l_{H_2O}/\lambda_{H_2O}) \\
&= \quad \text{survival probability through optical media} \\
P_{ri} \quad &= \quad \text{reflection probability at inner acrylic surface} \\
P_{ro} \quad &= \quad \text{reflection probability at outer acrylic surface} \\
\mathcal{R}(\hat{u}_p \cdot \hat{u}_i) \quad &= \quad \text{angular response of PMT/concentrator} \\
&\qquad \text{combination } \textit{not including solid angle}
\end{aligned}
$$

The l's are the photon path length in each medium and the λ's are the absorption length in each medium. The relation for the survival probability is true for any single wavelength, but because the spectral shape changes significantly over the path length of the light it is not possible to define a single absorption length for Cherenkov light in the SNO detector. The effective absorption length for acrylic, for instance, is about 12 cm for a 5 cm thick sheet and 18 cm for a 10 cm thick sheet, purely because of spectral shape changes. It is therefore necessary to determine the actual survival probability of any photon by integrating the absorption over the spectral shape. The same is true of the quantum efficiency, which is why it is shown as depending on the path length through each medium. Note that the lengths in each medium have to be corrected for refraction at the acrylic surfaces: this is the most tedious part of the calculation, and makes performing the sum over all PMTs extremely slow, taking several minutes per event.

Multiplying the mean number of photons emitted in the direction of PMT i by the detection probability gives the mean number of photons detected by

that PMT for the assumed event parameters:

$$N_d^i = P_d^i \times N_e^i \tag{3}$$

This value is used to calculate a log-likelihood for the event parameters according to:

$$L = - \sum_{j=unhit} \ln(\exp(-N_d^j)) - \sum_{k=hit} \ln((1 - \exp(-N_d^k \times 0.9973)) \tag{4}$$

where the factor 0.9973 accounts for the 3σ limits put on in-time light by the modal fitter (it is also possible to weight individual photons by a normalized Gaussian with a mean of zero and standard deviation of 1.6 ns to account for the arrival-time residual dt for each PMT, but as the modal fitter forces the arrival-time distribution to have this shape in any case, doing this adds no further information to the likelihood.)

The sums are over hit and unhit PMTs, so the likelihood is the joint probability of all PMTs that are not hit of not getting hit, and all the PMTs that are hit of getting hit. Calculating the likelihood in this way includes all the available information about the event with the important exception that scattered and reflected light is treated as "undetected". For events near the acrylic vessel (i.e. the vast majority of events) the role of reflected light in particular will be shown to significantly degrade this method of analysis by cutting down on the statistics of the event. However, it still may prove useful as a means of event-type-identification.

Note that for hit PMTs a minimum probability is artificially imposed on the algorithm, given by the noise rate: scattered or reflected photons that result in very low hit probabilities are assigned the probability arising from the noise rate and the $\pm$ 100 ns trigger window. Also, for the most precise correction the attenuation length and PMT efficiency will be included on a panel-by-panel or tube-by-tube basis, but this has not yet been done as it will be shown to be of questionable utility.

Although the algorithm was not used to fit the events, it was used to correct the direction of events to find the maximum likelihood. The time-consuming part of the calculation depends only on the position of the electron, not its energy or direction. The likelihood was therefore maximized by scanning over energy (from 1 to 20 MeV in 0.1 MeV steps) and finding the best direction for the best energy using the *Numerical Recipes* amoeba algorithm. This resulted in a small improvement over in the angular resolution over that given by the modal fitter alone: the improvement is comparable to

8

that given by the Circular Hough Transform correction described elsewhere [1].

A short test was run to see if the likelihood was likely to improve the fit over the modal fitter. As shown in Figure 9, the negative of the log-likelihood for the correct event position is generally greater than the value at the position found by the modal fitter. This means that it is unlikely fitting with the full likelihood would result in much improvement in the fit.

5 Results of Correcting for Optics and Geometry

The utility of the correction algorithm was tested by applying it to 7 MeV events uniformly distributed throughout the acrylic vessel. The calibration MC with an homogeneous acrylic vessel, no neck and uniform PMT response was used for the simulation. SNOMAN optical properties were used for the D_2O and H_2O , while the Chalk River measurements were used for the acrylic attenuation. Data from Robert Boardman's thesis were used for the PMT quantum efficiency. The PMT/concentrator model used was relatively simple and differed from the correct response significantly: this should not affect the results as the same response was used in the correction algorithm as the MC, and in any case the differences for events in the acrylic vessel are small.

The scale of the correction can been seen in Figure 10, which shows the response of the detector to 7 MeV electrons at the center and uniformly distributed throughout the acrylic vessel. The size of the shift and its direction depend on the choice of optical properties.

The results are disappointing: the correction works fairly well for events near the centre of the vessel, where the fraction of reflected light is only a few percent. But even in this case there is very little gain in the energy resolution. The predicted value of nhit for the parameters that give the maximum likelihood versus the actual value is shown in Figure 11. The agreement is quite good, but there is in fact a slight worsening of the resolution, particularly when compared with the resolution of the detector when run as a calorimeter (i.e. all light, not just in-time light, used to estimate the event energy.) The few points with very low predicted nhit come from events that are much nearer the acrylic vessel than the fit point. Only events fit inside of 550 cm were included in the analysis, but this includes a few that are actually very close to the acrylic vessel, where the correction is extremely sensitive to position due to the large coefficients of reflection at high incident angles on the acrylic.

9

Method	Resolution
All Hits	14.2%
In-Time Hits	15.2%
ML Hits	17.7%
ML Source	16.8%
ML Energy	14.1%

Table 5: SNO Detector Resolution for various ways of estimating event energy

The predicted energy peaks in the correct place, but the peak has a width of almost 1 MeV, for a resolution of 14.1%, which is just equal to the resolution obtained by simply counting hits. Table 5 shows the resolution for 7 MeV electrons using different methods of estimating the event energy or number of PMTs hit. The various maximum likliehood estimates are:

- ML Hits: the estimated number of hits for the energy and direction that gives the maximum likelihood

- ML Source: the estimated number of Cherenkov photons created by the event for the energy and direction that gives the maximum likelihood

- ML Energy: the energy that gives the maximum likelihood

6 Conclusion:

Preliminary comparisons between the three codes used to model the SNO detector show good agreement apart from differences in concentrator and PMT geometry. The concentrator geometry used in QMC is significantly different from the correct geometry, and this may effect the simulation of events in the H_2O . The angular distribution of Cherenkov photons has been found to depend on the EGS4 parameter ESTEPE, and work is underway to correct this problem.

An algorithm has been developed for correcting SNO events for optical and geometric effects. The relations for the correction are identical to those required for a maximum-likelihood fitter using all information about the event. The performance of the correction algorithm in preliminary tests is unpromising: the resolution for the corrected events is somewhat poorer than for the uncorrected events. The reasons for this are:

- Loss of statistics: Because only in-time light can be used by the correction algorithm there is about a 20% reduction in the number of photons in the event.

10

- Position sensitivity: The reflection co-efficients in particular are very sensitive to the position of the event, particularly for events near the acrylic vessel (i.e. the majority.)

- Angular distribution: The angular distribution of Cherenkov photons is not well-represented by the average behaviour. It has been shown by Ira Blevis et al at CRPP that single-electron events can be classified into 1, 2, 3 and > 3 ring events [2] with 20% in the first category, 70% in the second and the balance in the third and fourth. These distinct morphologies are averaged together into the angular distribution used by the correction algorithm, so it will not necessarily represent the angular distribution of any one event particularly well.

Given these problems it seems unlikely that this method of improving the resolution is worth pursuing further, although there is some promise that the algorithm may be useful in modeling high-energy events and in determining event type.

TABLE 1

	l.nm.(X)	n(Y)	atten(Y)	scat(Y)
1	200	1.41812	45.09109	900.58542
2	220	1.39712	103.78817	1323.9749
3	240	1.38259	207.25898	1882.7197
4	260	1.37218	370.48825	2603.8863
5	280	1.36447	606.1167	3561.8022
6	300	1.35861	922.34637	4776.8506
7	320	1.35404	1321.5860	6292.7564
8	340	1.35041	1800.0904	8087.6461
9	360	1.34746	2348.5902	10244.125
10	380	1.34503	2953.6847	12820.498
11	400	1.34299	3599.6381	15926.008
12	420	1.34126	4270.1549	19600.131
13	440	1.33977	4949.8750	23906.753
14	460	1.33847	5625.3711	28844.972
15	480	1.33734	6285.7205	34516.248
16	500	1.33633	6922.6079	41017.427
17	520	1.33543	7530.1993	48417.054
18	540	1.33462	8104.8061	56702.883
19	560	1.33389	8644.5127	65581.631
20	580	1.33322	9148.7516	75495.555
21	600	1.33261	9617.9870	86524.123
22	620	1.33205	10053.369	98813.552
23	640	1.33153	10456.529	112388.90
24	660	1.33105	10829.361	127330.77
25	680	1.33061	11173.891	143682.55
26	700	1.33019	11492.202	161440.34
27	720	1.3298	11786.317	180696.57
28	740	1.32943	12058.195	201626.12
29	760	1.32908	12309.689	224323.25
30	780	1.32876	12542.527	248884.77
31	800	1.32845	12758.303	275410.10

TABLE a

	1.nm.(X)	n(Y)	atten(Y)	scat(Y)
1	200	1.58101	0.20034	150000000
2	220	1.56487	0.26704	150000000
3	240	1.55222	0.3696	150000000
4	260	1.5421	0.54752	150000000
5	280	1.53385	0.93215	150000000
6	300	1.52704	2.38293	150000000
7	320	1.52135	8.63417	150000000
8	340	1.51654	16.92317	150000000
9	360	1.51245	30.7801	150000000
10	380	1.50893	52.56685	150000000
11	400	1.50589	85.09607	150000000
12	420	1.50325	131.57822	150000000
13	440	1.50093	195.54718	150000000
14	460	1.4989	280.77367	150000000
15	480	1.49709	391.17342	150000000
16	500	1.4955	530.71505	150000000
17	520	1.49407	703.3337	150000000
18	540	1.49279	912.85703	150000000
19	560	1.49165	1162.9330	150000000
20	580	1.49061	1456.9854	150000000
21	600	1.48968	1798.1634	150000000
22	620	1.48883	2189.3125	150000000
23	640	1.48806	2632.9589	150000000
24	660	1.48736	3131.2922	150000000
25	680	1.48672	3686.1628	150000000
26	700	1.48613	4299.1017	150000000
27	720	1.48559	4971.2895	150000000
28	740	1.4851	5703.6137	150000000
29	760	1.48464	6496.6586	150000000
30	780	1.48422	7350.7267	150000000
31	800	1.48383	8265.8666	150000000

TABLE 3

	l.nm.(X)	n(Y)	atten(Y)	scat(Y)
1	200	1.41812	300.77189	547.15296
2	220	1.39712	394.01751	930.95589
3	240	1.38259	538.8658	1467.7125
4	260	1.37218	765.94956	2187.0481
5	280	1.36447	1133.7692	3121.2384
6	300	1.35861	1757.9471	4305.4028
7	320	1.35404	2875.2457	5777.5837
8	340	1.35041	4953.4948	7578.7736
9	360	1.34746	8588.8177	9752.9177
10	380	1.34503	12618.450	12346.908
11	400	1.34299	12444.166	15410.579
12	420	1.34126	8953.5374	18996.695
13	440	1.33977	5997.5190	23160.946
14	460	1.33847	4161.8867	27961.944
15	480	1.33734	3047.7015	33461.218
16	500	1.33633	2342.5335	39723.211
17	520	1.33543	1873.0565	46815.278
18	540	1.33462	1545.7354	54807.681
19	560	1.33389	1308.3899	63773.595
20	580	1.33322	1130.5084	73789.098
21	600	1.33261	993.45147	84933.179
22	620	1.33205	885.35377	97287.732
23	640	1.33153	798.37955	110937.55
24	660	1.33105	727.19509	125970.35
25	680	1.33061	668.0643	142476.73
26	700	1.33019	618.30679	160550.22
27	720	1.3298	575.9582	180287.23
28	740	1.32943	539.55127	201787.10
29	760	1.32908	507.97044	225152.04
30	780	1.32876	480.35573	250487.20
31	800	1.32845	456.03399	277900.62

7 Figure Captions

Figure 1: D_2O attenuation length estimated from White Book extinction data for the three Monte Carlos

Figure 2: Acrylic attenuation length estimated from White Book extinction data for the three Monte Carlos

Figure 3: H_2O attenuation length estimated from White Book extinction data for the three Monte Carlos

Figure 4: SNOMAN, QMC and calibration MC concentrator shapes. The original QMC shape is somewhat longer than that shown here.

Figure 5: Deviation between calibration MC concentrator shape and SNOMAN concentrator shape.

Figure 6: Comparison between measured concentrator/PMT response and calibration MC calculated response.

Figure 7: Number of photons produced as a function of $\cos\theta$ and electron energy for ESTEPE = 0.05

Figure 8: Number of photons produced as a function of $\cos\theta$ and electron energy for ESTEPE = 0.01

Figure 9: Effect of optics and geometry on detector resolution. The resolution for a source at the centre is the best possible. The direction of the shift in the peak for a distributed source, and the width of the peak, is a function of the optical parameters modeled.

Figure 10: Negative log-likelihood for the true position and the fitted position. The line has a slope of one and passes through the origin. Points above the line have have a higher likelihood (lower negative log-likelihood) for the fitted point than the true point.

Figure 11: Maximum likelihood estimate of number of hits for the fit position and the best direction and energy for 7 MeV electrons uniformly in the D_2O .

Figure 12: Maximum likelihood estimate of the energy of 7 MeV electrons uniformly in the D_2O .

References

[1] T. J. Radcliffe, SNO-STR-94-019, Pattern Recognition for Event-Type Identification in the SNO Detector

[2] I. Blevis, F. Dalnoki-Veress, C. Hargrove, Charge Current Event Topology
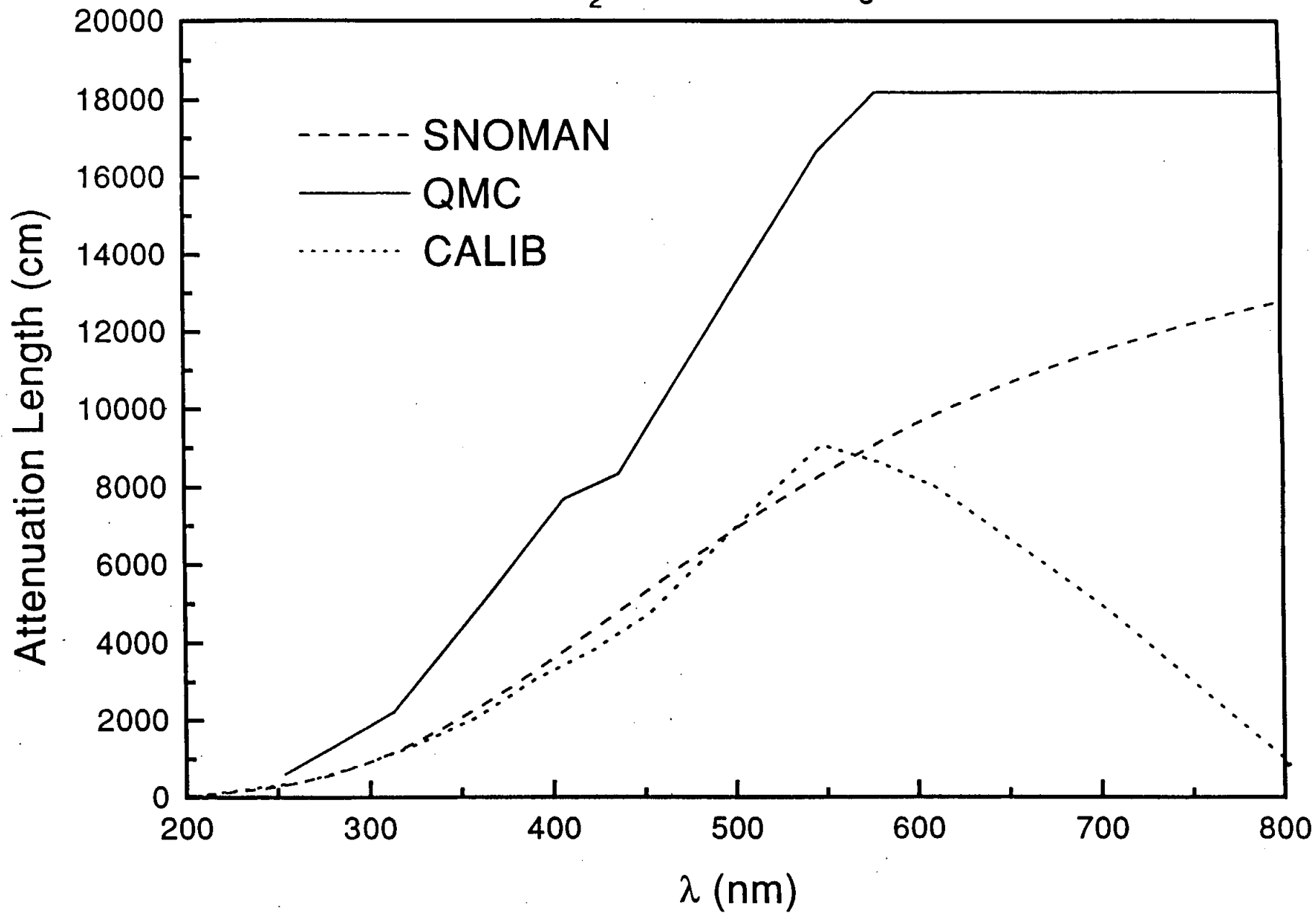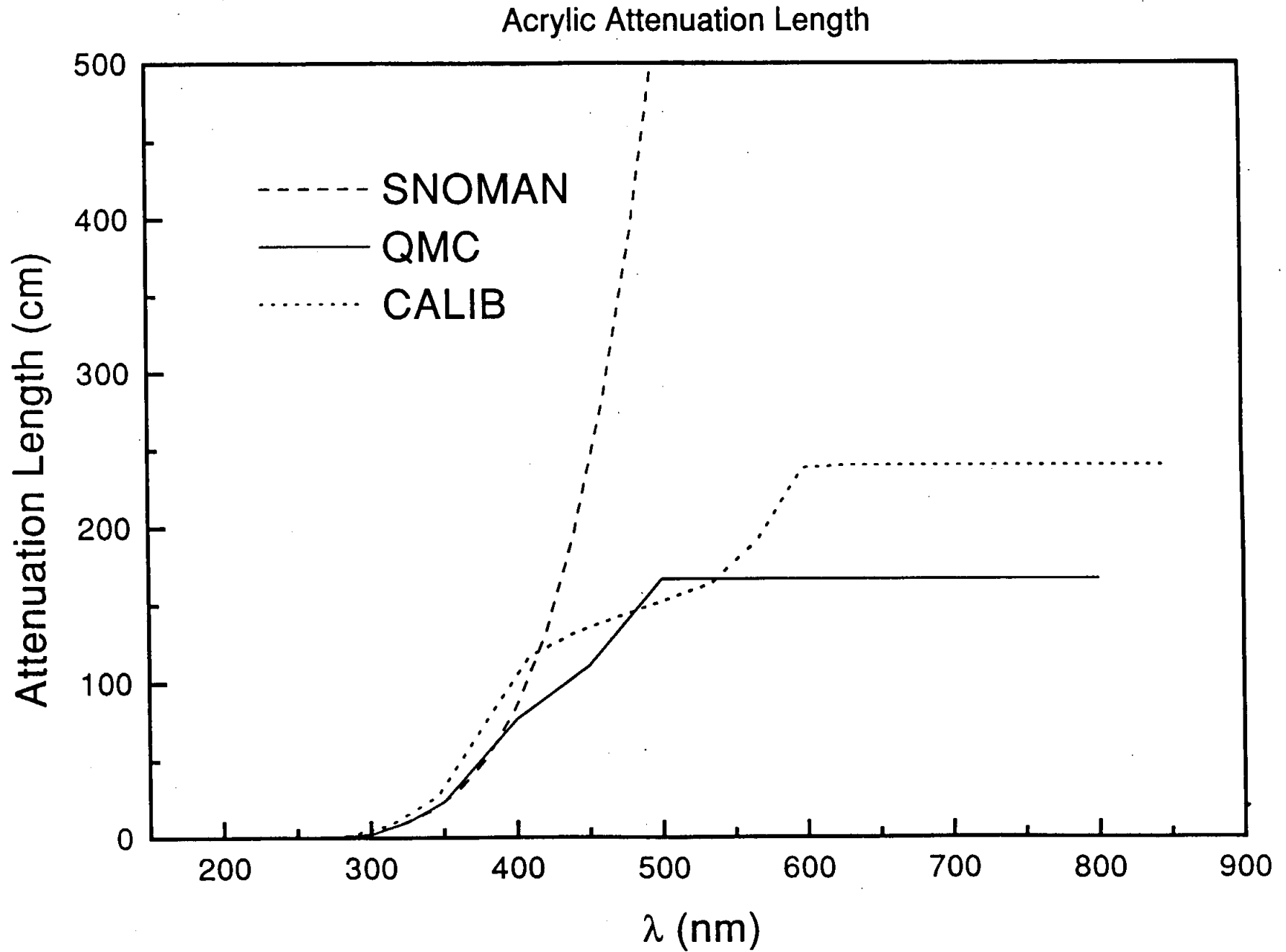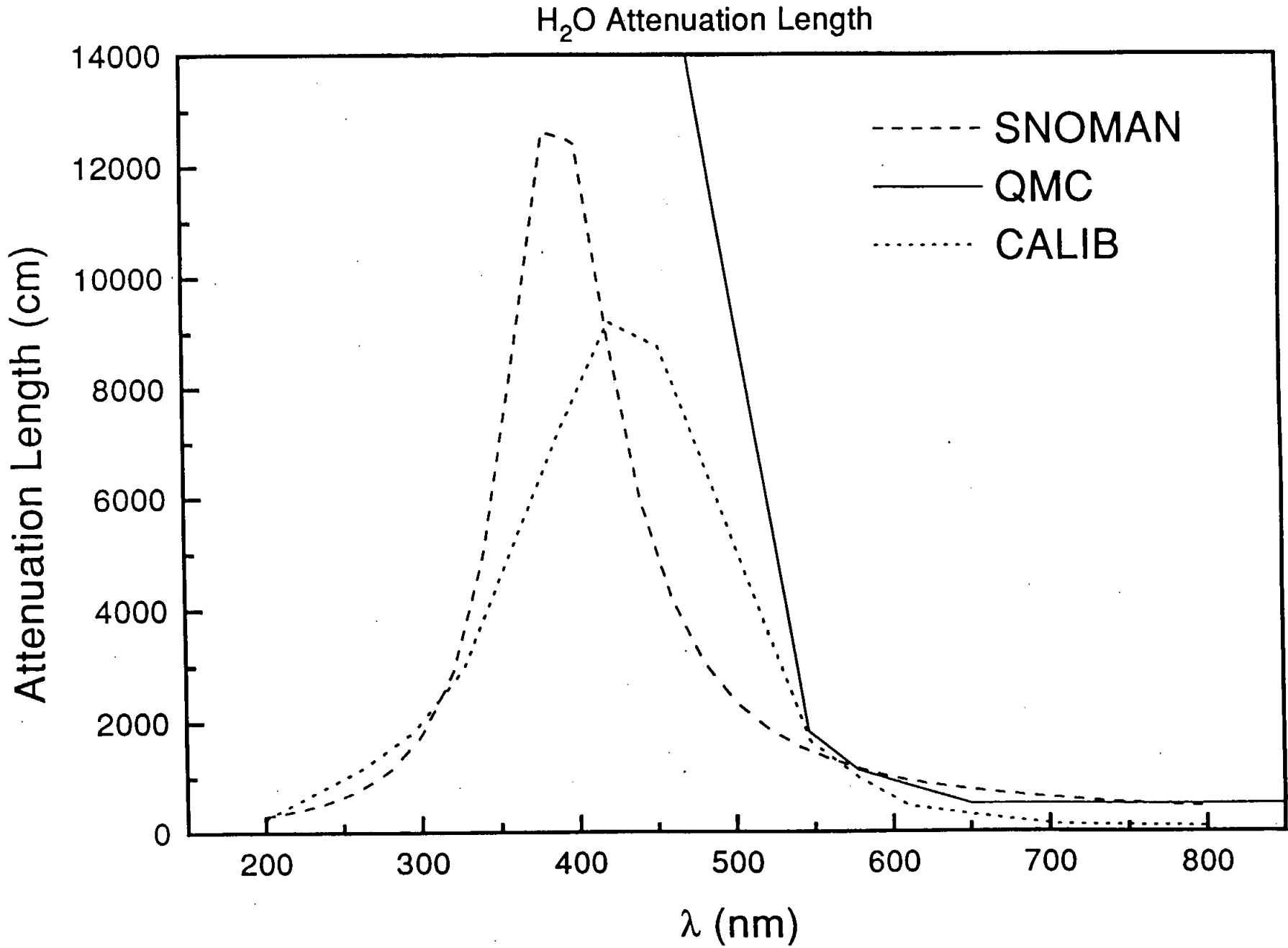
FIG. 1

D$_2$O Attenuation Length

SNOMAN
QMC
CALIB

Attenuation Length (cm)

λ (nm)

Fig. 2

Acrylic Attenuation Length

H₂O Attenuation Length

Legend:
- SNOMAN (dashed)
- QMC (solid)
- CALIB (dotted)

Y-axis: Attenuation Length (cm)

X-axis: λ (nm)

FIG. 4

Concentrator Shapes

— SNOMAN SHAPE
······ QMC SHAPE
—○— CALIBRATION SHAPE

Concentrator Radius (cm)
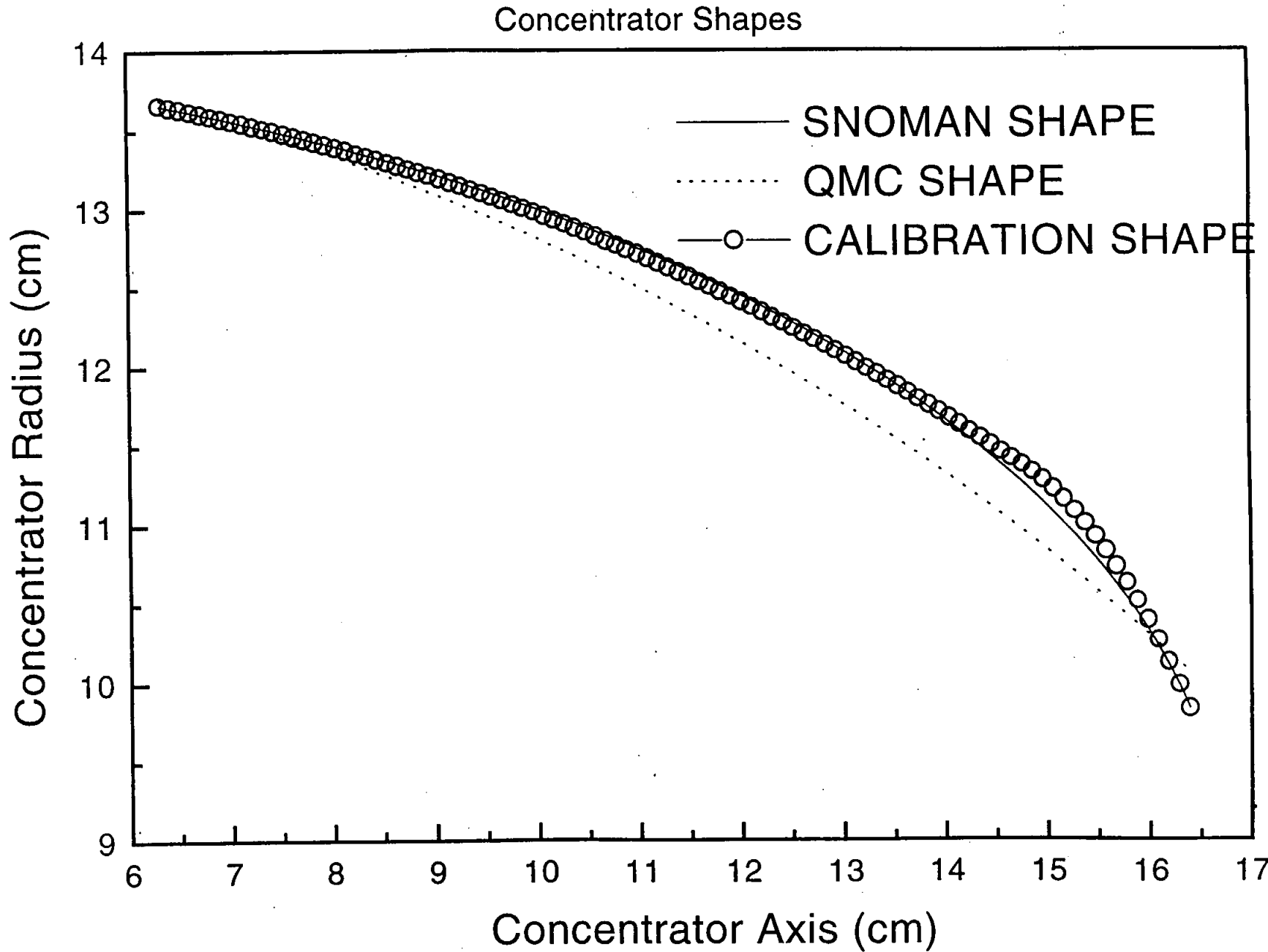
Concentrator Axis (cm)
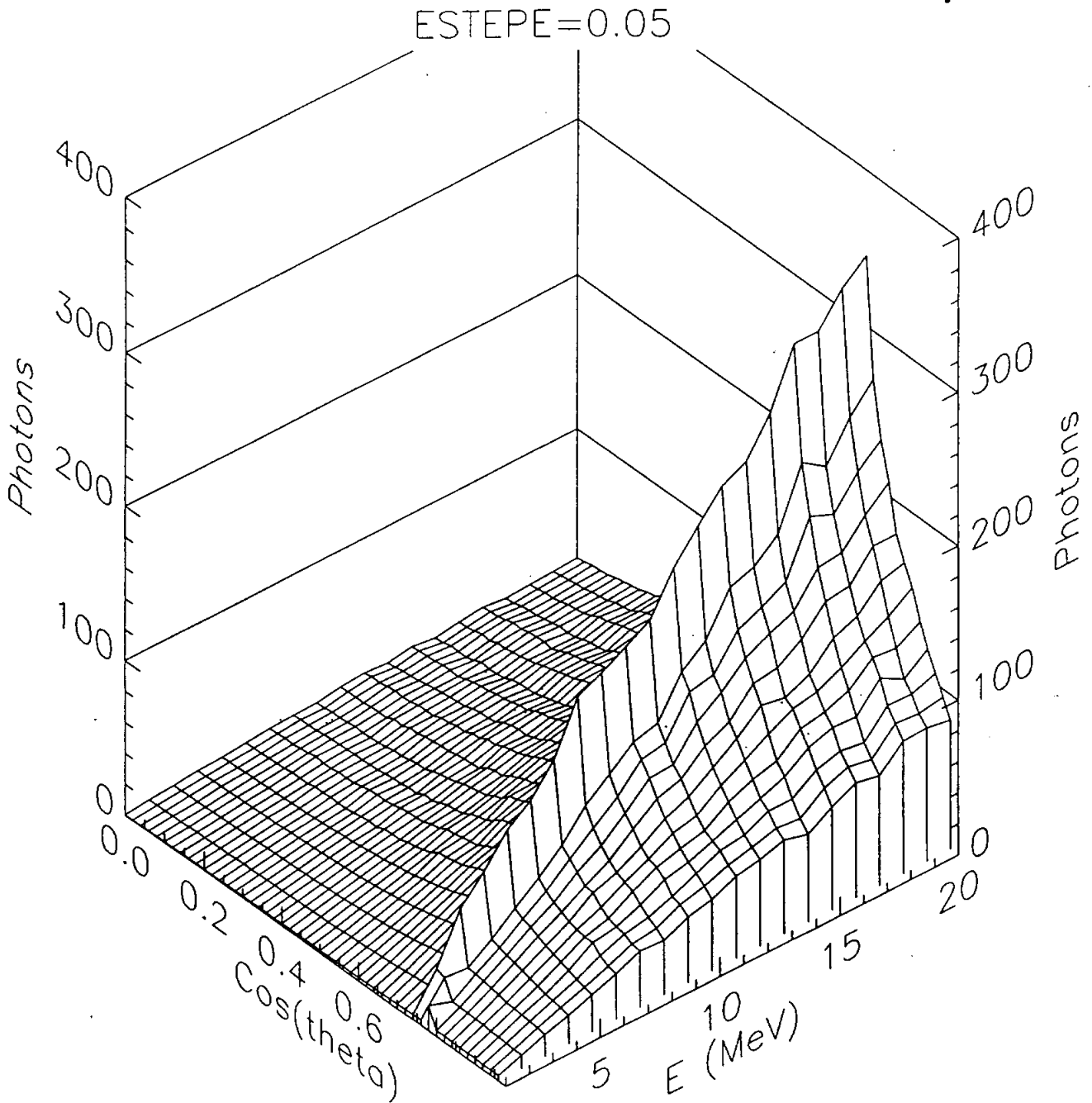
Difference Between SNOMAN and CALIBRATION Concentrator Shapes
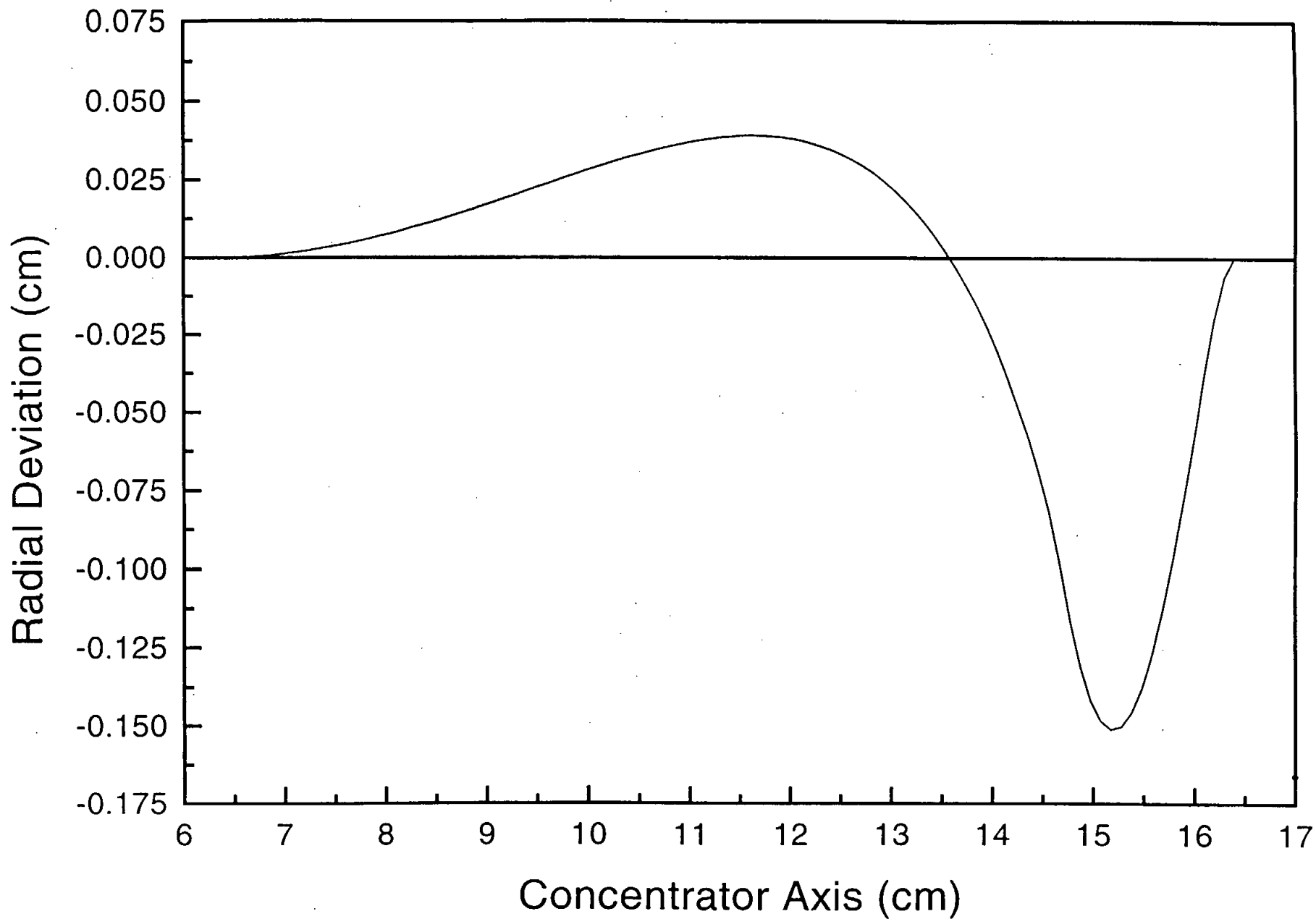
FIG.6

Comparison of GMC and Measured PMT Angular Response

Angle (degrees)

ESTEPE=0.05

Photons

400

300

200

100

0

0.0

0.2

0.4

0.6

Cos(theta)

5

10

15

20

E (MeV)

400

300

200

100

0

Photons
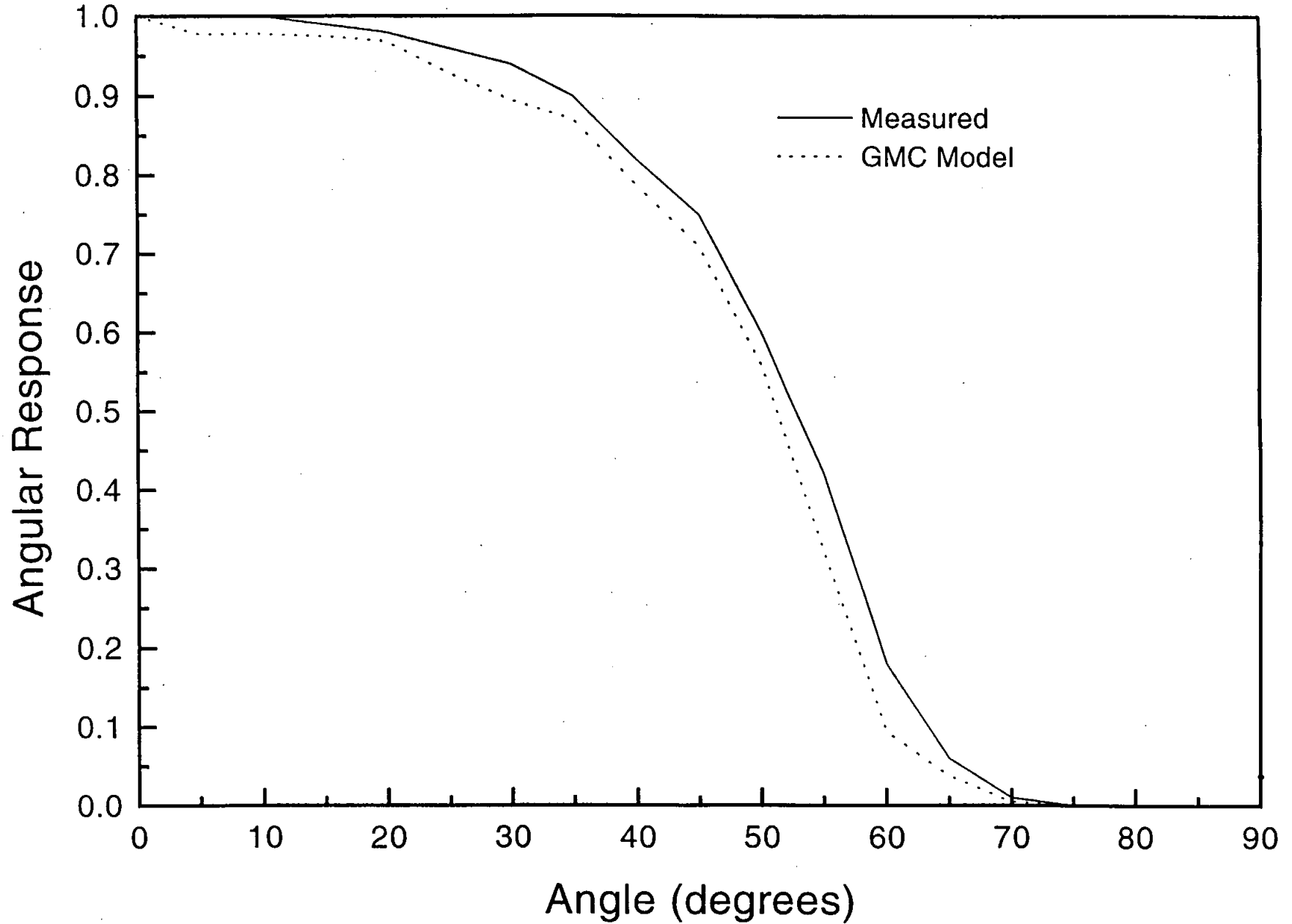
FIG. 1

ESTEPE=0.01
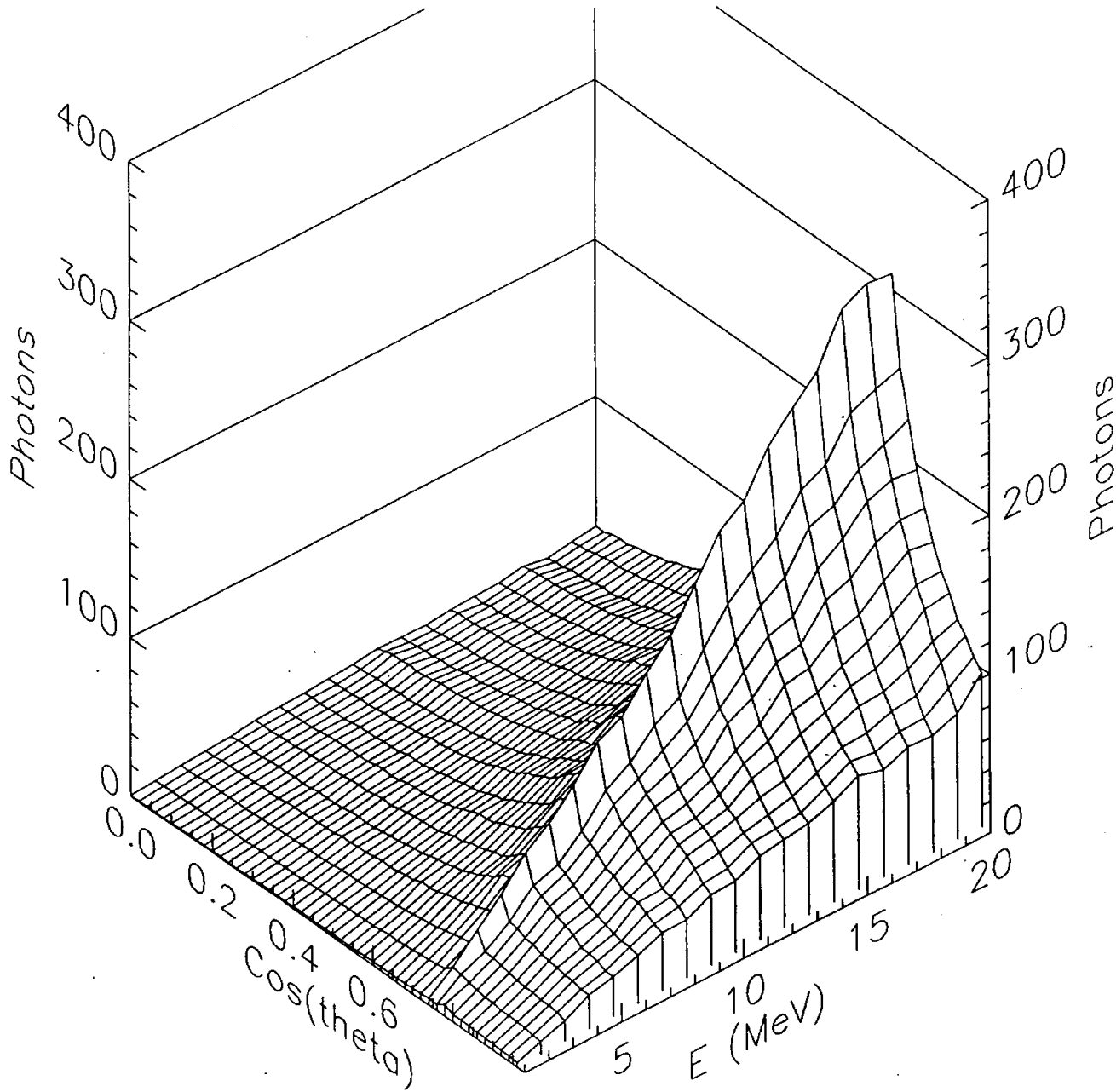
FIG. 8

Fig.

7 MeV e⁻ at Centre and Uniformly in Vessel: Calibration MC

Centre (mean = 65.184 σ = 10.71)
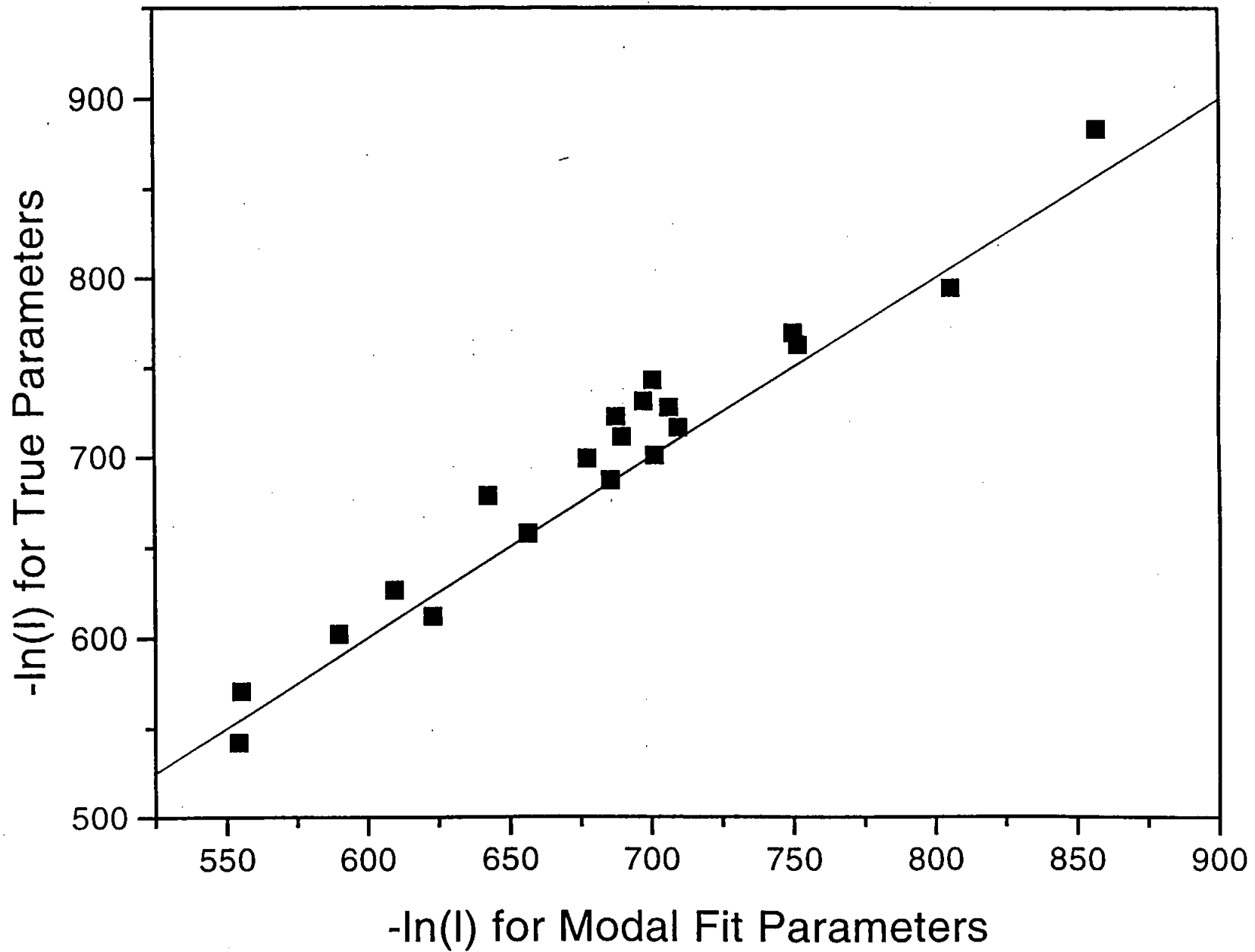Uniform (mean = 77.106 σ = 14.16)
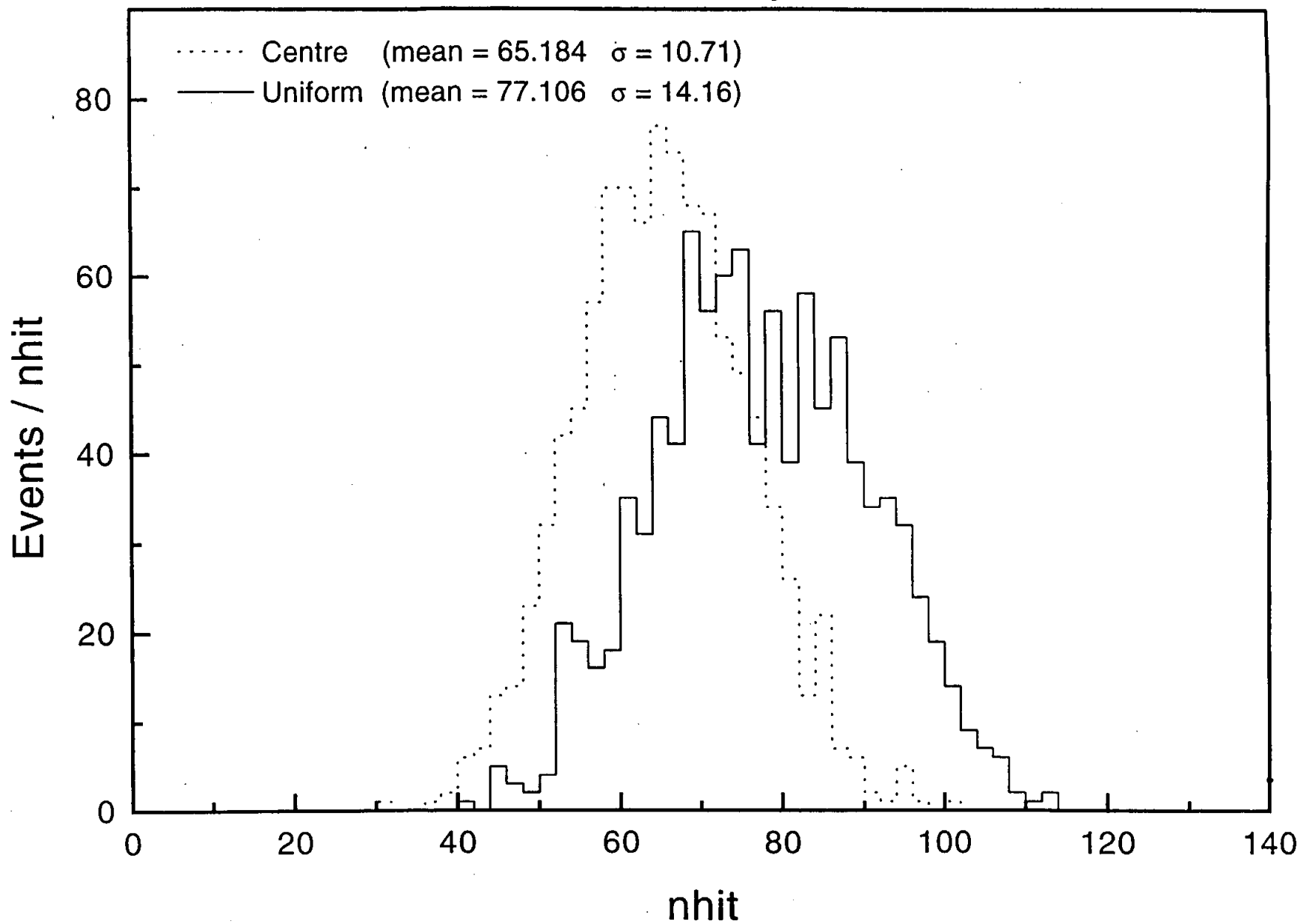
FIG. 10

Angle and Energy Likeliehood vs. Modal Fitter
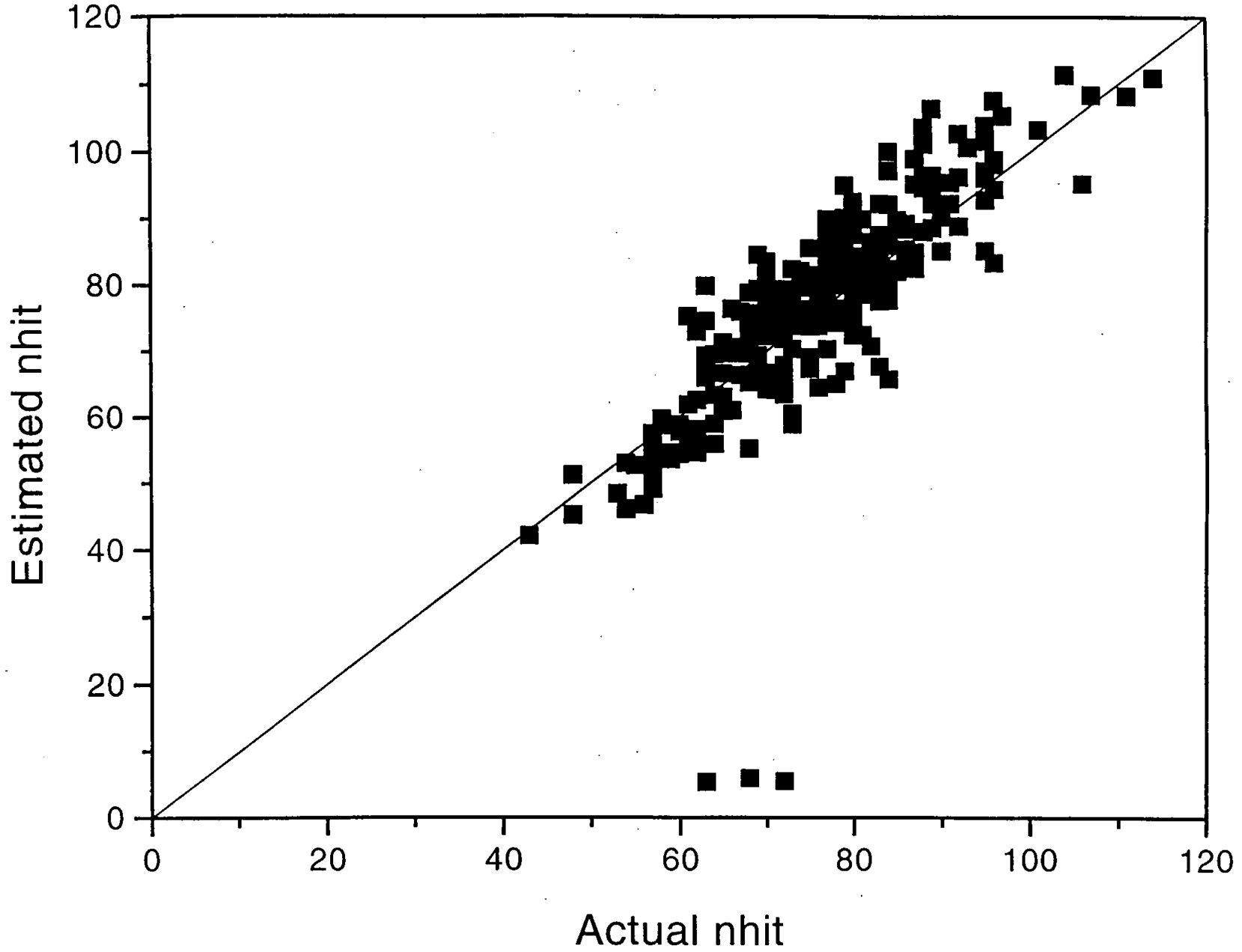
FIG. 1

Maximum Likeliehood Estimate vs. Actual nhit

FIG. 12

Maximum Likeliehood Estimate of Energy for 7 MeV e⁻

Mean = 6.89587 +/- 0.066525

σ = 0.97472 +/- 0.062830

Energy (MeV)